J Mater Sci (2007) 42:5973–5981
DOI 10.1007/s10853-006-1111-7

Influence of the submerged arc welding in the mechanical behaviour of the P355NL1 steel—part II: analysis of the low/high cycle fatigue behaviours

Abilio Manuel Pinho De Jesus · Alfredo S. Ribeiro · Antonio A. Fernandes

Received: 25 August 2005 / Accepted: 6 October 2006 / Published online: 6 April 2007

Abstract A normalized fine grain carbon low alloy steel, P355NL1 (EN10028-3), intended for service in welded pressure vessels, where notch toughness is of high importance, has been investigated. Applications with this steel usually require the intensive use of welds. One of the most common welding processes that are used in the manufacturing of pressure vessels is the submerged arc welding. This welding process is often automated in order to perform the main seam welds of the body of the vessels. The influence of the automated submerged arc welding, in the mechanical performance, is investigated. In this paper (Part II) the low and high cycle fatigue and crack propagation behaviours are compared between the base and welded materials. Several series of small and smooth specimens as well as cracked specimens made of base, welded and heat affected materials, respectively, were fatigue tested. Strain, stress and energy based relations for fatigue life assessment, until crack initiation, are evaluated based on experimental results and compared between the base and welded materials. Finally, the fatigue crack propagation behaviours are compared between the base, welded and heat affected materials.

A. M. P. De Jesus (✉) · A. S. Ribeiro
Department of Engineering, University of Tras-os-Montes and Alto Douro, Quinta de Prados, 5001-801 Vila Real, Portugal
e-mail: ajesus@utad.pt

A. A. Fernandes
DEMEGI – Faculty of Engineering,
Universtiy of Porto,
Rua Dr. Roberto Frias, 4200-465 Porto, Potugal

Introduction

Pressure vessels are an important type of structures that usually experience, during operation, cyclic loads that lead to fatigue failures [1]. The design of this equipment should take into account all foreseeable degradation mechanisms, including fatigue. The need for inclusion of a fatigue assessment route in design of pressure equipment has been enforced by some important organizations [2]. It is a common industrial practice to use specific design codes such as the ASME VIII – Div. 2 [3], the PD5500 [4] and the recently approved EN 13445 [5]. Alternative, more general and flexible procedures exist such as the local approaches [6, 7] or the Fracture Mechanics [8–10] that can be used to model fatigue for both welded and unwelded structural details. The authors have developed important experimental investigations on the P355NL1 steel [11]. This material is well suited for pressure vessels industry, where high toughness and weldability are essential characteristics.

Now, the authors propose in two papers (Part I and Part II) a comparison of the mechanical behaviour between the P355NL1 steel—base material (BM)—and the welded material (WM), resulting from the submerged arc welding process, which is a very important welding process in the manufacturing of pressure vessels. In this paper (Part II), the low and high cycle fatigue behaviours (fatigue resistances) are evaluated and compared between the BM and the WM. Strain-life, stress-life and energy-life experimentally based relations are proposed for those materials. Additionally, crack growth rates are determined for the BM, WM and for the material affected by the heat introduced by the welding process (HAZ).

The information included in this paper (Part II) is complemented with the information incorporated in a Part I

paper [12]. The latter paper describes and compares the cyclic elastoplastic behaviours between the BM and WM. Detailed information about the static strength properties, chemical composition and microstructures of the BM and WM are also reported in the Part I paper [12]. The research documented in both papers is of extreme importance if a local approach to fatigue or a Linear Elastic Fracture Mechanics (LEFM) approach have to be applied, separately or in conjunction, to assess the main welds of pressure vessels.

Local approaches to fatigue

The local approaches constitute a very important methodology for the assessment of the fatigue behaviour of structural components. They are usually used to model the initiation of fatigue cracks. They are based on the hypothesis that the behaviour of the material, in a critical location of a structural component, can be described using data from smooth specimens. The data obtained from the test of smooth specimens can be presented in several forms. The most common data is the strain-life data. Alternative data can also be proposed such as stress-life and energy-life data. Some relations for these three alternative forms are described in the next subsections.

Strain-life relations

Strain-life relations are mainly proposed to describe low cycle fatigue results. Typical relations have been suggested to correlate the cyclic strain amplitude with the number of reversals to failure, $2N_f$, usually considered to correspond to the initiation of a macroscopic crack (crack depth of 0.25 mm). The most used relation to model low cycle fatigue was proposed by Coffin [13] and Manson [14], which relates the plastic strain amplitude, $\Delta\varepsilon^p/2$, with the number of reversals to crack initiation, $2N_f$:

$$\frac{\Delta\varepsilon^p}{2} = \varepsilon'_f \left(2N_f\right)^c \tag{1}$$

where ε'_f and c are constants, respectively, the fatigue ductility coefficient and exponent. The Coffin-Manson relation can be extended to high cycle fatigue domains using the relation proposed by Basquin [15]. This relation relates the elastic strain amplitude, $\Delta\varepsilon^e/2$, with the number of reversals to crack initiation, $2N_f$:

$$\frac{\Delta\varepsilon^e}{2} = \frac{\Delta\sigma}{2E} = \frac{\sigma'_f}{E}\left(2N_f\right)^b \tag{2}$$

where σ'_f is the fatigue strength coefficient, b is the fatigue strength exponent, E is the Young modulus and $\Delta\sigma/2$ is the stress amplitude. The number of reversals, $2N_T$, corresponding to the transition between low and high cycle fatigue regimes is characterized by total strain amplitude, $\Delta\varepsilon_T/2$, composed by equal components of elastic and plastic strain amplitudes; lives below this transition value are dictated by ductility properties; lives above this transition value are dictated by strength properties. Morrow [16] suggested the superposition of Eqs. 1 and 2, resulting a more general relation, valid for low and high cycle fatigue regimes:

$$\frac{\Delta\varepsilon}{2} = \frac{\Delta\varepsilon^e}{2} + \frac{\Delta\varepsilon^p}{2} = \frac{\sigma'_f}{E}\left(2N_f\right)^b + \varepsilon'_f\left(2N_f\right)^c \tag{3}$$

where $\Delta\varepsilon/2$ represent the total strain amplitude.

Stress-life relations

Stress-life relations are used to correlate fatigue data obtained with fatigue tests of smooth specimens tested under stress control. Stress-life relations have been proposed mainly to assess high cycle fatigue. The Basquin relation (2) can be used in the form of a stress-life relation to model high cycle fatigue. Although being not consensual, some authors have proposed more sophisticated stress-life relations in order to model both low and high cycle fatigue regimes. An example of this type of relations was proposed by Lemaitre and Chaboche [17]:

$$N_f = \frac{\sigma_{\mathrm{UTS}} - \sigma_{\max}}{\sigma_{\max} - \sigma_l(\sigma_{\mathrm{med}})}\left(\frac{\sigma_{\max} - \sigma_{\mathrm{med}}}{B_0(1 - \beta\sigma_{\mathrm{med}})}\right)^{\eta} \tag{4}$$

where $\sigma_{\max}$ and σ_{med} are, respectively, the maximum and mean controlled stresses of the cycle, σ_{UTS} is the ultimate tensile strength, B_0 and η are constants to be determined by fitting Eq. 4 to the experimental results of fully-reversed tests and $\sigma_l(\sigma_{\mathrm{med}})$ is the endurance fatigue limit for non null mean stress. The endurance fatigue limit $\sigma_l(\sigma_{\mathrm{med}})$ can be determined using a modified form of Goodman's equation [17]:

$$\sigma_l(\sigma_{\mathrm{med}}) = \sigma_{\mathrm{med}} + \sigma_{l0}(1 - \beta\sigma_{\mathrm{med}}) \tag{5}$$

where σ_{l0} is the endurance fatigue limit for a fully-reversed loading and β, which also appears in Eq. 4, is the slope of the assumed linear relation between the endurance fatigue limit and the mean stress. The endurance fatigue limits are expressed in the form of a maximum stress of the cycle. Equation 4 was proposed to describe the complete Woehler curves, from the static rupture to the domain of fatigue endurance limits. It also describes the effect of the mean stress on the complete Woehler curves, including the mean stress effect on the fatigue endurance limits.

Energy-life relations

Stress-life and strain-life relations can be considered as classical or traditional local approaches. Modern local approaches have been proposed based on energy considerations, leading to the so-called energy-life relations. The energy-life relations have been intensively investigated by several authors such as Halford [18], Lefebvre and Ellyin [19], Ellyin and Kujawski [20], Golos and Ellyin [21] and Ellyin [22]. The energy-life relations can be formulated using the following general form, proposed by Ellyin [22]:

$$\psi = k(2N_f)^{\alpha} + \psi_0 \tag{6}$$

where ψ is an energy-based damage parameter, ψ_0 is an energy-based endurance fatigue limit, k ($k > 0$) and α ($\alpha < 0$) are constants resulting from the best fitting of Eq. 6 to the experimental results.

Three common forms of energy-based damage parameters are the plastic strain energy density, the total strain energy density and a modified total strain energy density that takes into account the effect of the mean stress. The plastic strain energy density per cycle, ΔW^p, corresponds to the area of the hysteresis loops which, for a non-Masing material, has the following form [19, 20]:

$$\Delta W^p = \frac{1-n^*}{1+n^*}\Delta\sigma\Delta\varepsilon^p + \frac{2n^*}{1+n^*}\delta\sigma_0\Delta\varepsilon^p \tag{7}$$

where $\delta\sigma_0$ is the increase in the proportional stress limit that can be calculated using Eqs. 1–3 presented in the Part I paper [12], n^* is the strain-hardening exponent of the master curve also defined in [12]. The total strain energy density per cycle, ΔW, is given by the following formula:

$$\Delta W = \frac{1}{2}\Delta W^p + \frac{1}{2}\Delta\sigma\Delta\varepsilon \tag{8}$$

The energy-based parameters ΔW and ΔW^p are suitable only for fully- or almost fully-reversed tests, because they are not sensitive to the mean stress. Golos and Ellyin [21] proposed another version of total strain energy density, ΔW^t, in order to be sensitive to the mean stress. This energy is equal to the plastic strain energy density, defined in Eq. (7), plus the elastic strain energy density associated to the tensile stress of the cycle, ΔW^{e+}, defined as follows:

$$\Delta W^{e+} = \frac{1}{2E}\left(\frac{\Delta\sigma}{2} + \sigma_{\text{med}}\right)^2 = \frac{\sigma_{\max}^2}{2E} \tag{9}$$

Fracture Mechanics approach

The Fracture Mechanics approach can be used as an alternative to the local approaches [9, 10]. This approach is based on the pre-existence of a small defect or flaw which is assumed to be an initial crack. Fracture Mechanics models the propagation of fatigue cracks from an initial size to final dimensions responsible for the fracture of structural components. Fracture Mechanics can also be used to complement the local approaches [8, 23]. Local approaches are used to model the initiation of a macroscopic crack and Fracture Mechanics approaches are used to model the propagation of the initial macroscopic crack until rupture occurs. Thus, the total number of cycles to ultimate failure, N_f, can be expressed as follows:

$$N_f = N_i + N_P \tag{10}$$

where N_i is the number of cycles required to initiate a crack and N_P is the number of cycles required to propagate the crack.

The LEFM is a well established branch of Fracture Mechanics that has been applied intensively to the propagation period of fatigue cracks [24]. The LEFM is based on the hypothesis that the stress intensity factor, K, is the mechanical parameter that controls the stress range at the crack tip. Several laws have been proposed to characterize the fatigue crack propagation rates, combining the da/dN and ΔK parameters. A well known classical relation was proposed by Paris et al. [25, 26] and has the following form:

$$\frac{da}{dN} = C(\Delta K)^m \tag{11}$$

where da/dN is the fatigue crack propagation rate, $\Delta K = K_{\max} - K_{\min}$ represents the range of the stress intensity factor and C and m are material constants. Walker [27] proposed a modification to the Paris's law in order to take into account the mean stress effect:

$$\frac{da}{dN} = C\left[/(1-R_\sigma)^{1-\lambda}\right]^m \tag{12}$$

where C and m are the constants of the Paris's law for a stress ratio, $R_\sigma = -1$; λ is a constant that allows the correlation of crack propagation data for several stress ratios. Many other relations have been proposed [28], but due to its simplicity and reasonable domain of applicability, the Paris's relation is widely applied.

Materials characterization and experimental details

This paper (Part II) presents experimental fatigue data obtained for the carbon low alloy steel P355NL1, delivered in the form of plates with 5.1 mm thickness. This designation is according to the EN10028-3 standard

[29]. This steel has the former designation of TStE355, specified in the DIN 17102 standard [30]. This steel is a weldable normalized fine grain structural steel, applied for pressure vessel purposes with special requirements for low temperatures. Materials resulting from the automated submerged arc welding are also investigated, namely the WM and the HAZ. The fatigue behaviours of these materials are compared based on an experimental program. Details about the studied materials can be found on the Part I paper [12]. Table 1 summarizes some important mechanical properties of the investigated materials derived in reference [12]. It is included the ultimate tensile strength and the cyclic yield stress of the BM and WM as well as the Vickers Hardness of the BM, WM and HAZ. The cyclic yield stress corresponds to a 0.1% permanent strain. The three materials are characterized by different microstructures and grain sizes [12] which are responsible for different hardness values, yield limits and crack initiation and propagation resistances.

Fatigue tests were performed on smooth and small specimens manufactured according to the ASTM E606 standard [31]. A total of nine series of specimens were tested, four under strain control ($2 \times R_\varepsilon = -1$, $2 \times R_\varepsilon = 0$) and five under stress control ($2 \times R_\sigma = -1$, $R_\sigma = -0.5$, $2 \times R_\sigma = 0$), resulting in a total of 127 tested specimens. Five series of specimens are made of BM; four series have WM at the gauge length. Details about the preparation of these specimens, descriptions of the series and fatigue tests are addressed in the Part I paper [12].

This paper also presents results from fatigue crack propagation tests conducted on cracked specimens using the compact tension (CT) geometry. The geometry and test procedures were defined according to the ASTM E647 standard [32]. The specimens were prepared in order to present BM, WM and HAZ on the crack path. Thus, crack propagation behaviours will be assessed for the referred materials. The CT specimens have a width, L, equal to 50 mm and a height, H, equal to 48 mm. The thickness of the specimens was 4.35 mm. A total of 14 specimens were tested under pulsating stress covering the stress ratios, $R_\sigma = 0$, $R_\sigma = 0.5$ and $R_\sigma = 0.7$ and the three materials.

Table 1 Mechanical properties of the BM, WM and HAZ

Materials	σ_{UTS} (MPa)	σ_y' (MPa)	HV10
BM	568	324	149
WM	585	418	158
HAZ	–	–	172

Results and discussion

Strain-life relations

Figures 1–3 present the strain-life data obtained in this research: Fig. 1 presents the total strain vs. life data; Fig. 2 presents the plastic strain vs. life data and Fig. 3 presents the elastic strain vs. life data. The data was obtained for the BM—the P355NL1 steel—and also for the WM. Two strain ratios were investigated. The analysis of the data shows that the two materials have similar fatigue strength behaviours as revealed by the elastic strain vs. life data. The plastic strain vs. life data shows distinct fatigue ductility behaviours of the BM and WM. The effect of the strain ratio on the strain-life data is negligible for the BM. This is explained by the complete cyclic mean stress relaxation observed for tests conducted under null strain ratio. The WM exhibits a strain-life behaviour which slightly depends on the strain ratio. This is due to the fact that, in general, the WM exhibits higher resistance to cyclic mean stress relaxation than BM, in particular for tests conducted under null strain ratio. The higher resistance of the WM to cyclic mean stress relaxation can be justified by its lower transition life as discussed hereafter.

Table 2 presents the constants for the strain-life Eq. 3. These constants were derived for $R_\varepsilon = -1$ and $R_\varepsilon = 0$ and also for the conjunction of both data. Constants are proposed for the BM and WM. The correlations coefficients, R^2, are also included in the Table 2. The number of cycles corresponding to the transition between the fatigue behaviour governed by ductility and the fatigue behaviour governed by strength properties are also included in Table 2. It can be observed that the BM presents a transition number of cycles about ten times higher than the WM. For the WM the strength properties are dominant for a wider fatigue range than that observed for the BM. This is consistent with the observation that the transition fatigue life decreases with increasing hardness for steels. The WM presents higher hardness than the BM as indicated in Table 1 which justifies the significant differences in the strain-life relations.

The strain-life data presented in this paper was derived for stabilized cyclic conditions of the BM and WM. Objectively, the strain-life data was established based on half-life data of the materials. As reported by authors on reference [12], the BM and WM exhibit distinct cyclic elastoplastic behaviours. While the BM stabilizes for high strain ranges, after an initial cyclic hardening, the WM did not show a stabilized behaviour for high strain ranges – the WM first cyclic hardens followed by cyclic softening until failure. For low strain ranges, the WM achieves a stabilized behaviour earlier than the BM. The cyclic softening is responsible for a reduction in the radius of the yield surface

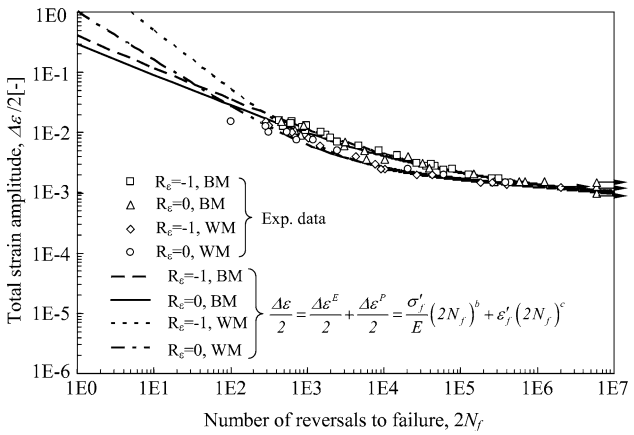

Fig. 1 Comparison of total strain-life data between the BM and WM

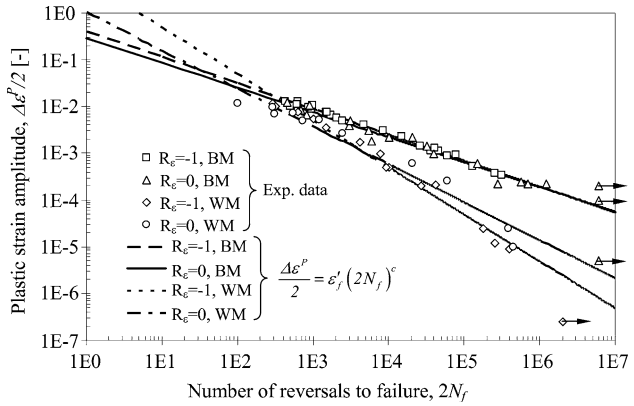

Fig. 2 Comparison of plastic strain-life data between the BM and WM

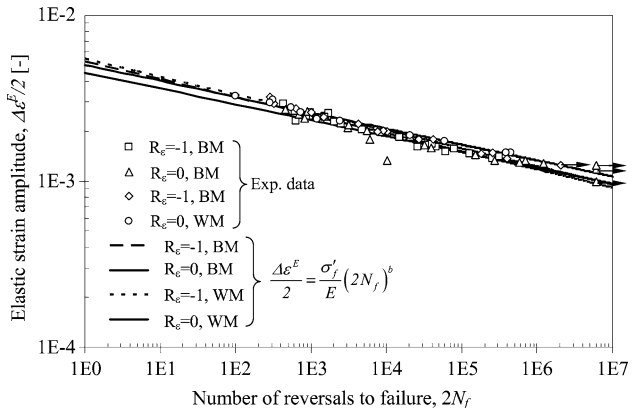

Fig. 3 Comparison of elastic strain-life data between the BM and WM

of the materials, contributing to increase the ductility properties of the material; inversely the cyclic hardening enlarge the radius of the yield surface of the material which contributes to increase the fatigue strength of the materials.

Stress-life relations

This paper also reports fatigue tests of smooth specimens carried out under stress control. Three stress ratios were tested for the BM ($R_\sigma = -1$, $R_\sigma = -0.5$ and $R_\sigma = 0.0$); two stress ratios were investigated for the WM ($R_\sigma = -1$ and $R_\sigma = 0.0$). Figure 4 presents all experimental data. The same figure also includes the curves obtained by the best fit of Eq. 4 to the experimental data. Table 3 summarizes the constants resulting from the referred curve fitting. It can be concluded that the expression proposed by Lemaitre and Chaboche [17] gives an overall good description. Although some difficulties are encountered in the description of the Woehler's curves, in particular for the low cycle fatigue domain, with $R_\sigma = 0$, the mean stress effect is reasonably captured by the model as well as the static rupture and the fatigue endurance asymptotes. Is more or less well established that the low cycle fatigue region is best described using strain-life relations rather than stress-life relations. The analysis of the data reveals that WM is more influenced by the mean stress than the BM, for high cycle fatigue. In fact, the S–N curves of the WM enclose the S–N curves of the BM which makes the WM more mean stress sensitive. A possible explanation for this observation is the fact that the WM has a significantly lower transition life than the BM which difficult the mean stress relaxation for medium/high cycle fatigue.

Energy-life relations

Figure 5 illustrates the energy-life relations obtained for the BM and WM, using the damage parameters described in Eqs. 7–9. The endurance fatigue limits are defined as being the energy leading to two million reversals of failure. The proposed energy-life relations were derived from the strain-life data obtained for $R_\varepsilon = -1$. The proposed energy-life relations are in close agreement with the experimental data. Table 4 summarizes the constants of the energy-life Eq. 6. In general, WM exhibits lower fatigue resistance than BM. This difference is much more pronounced if the plastic strain energy density is used as a damage parameter. The difference is minimal if the total strain energy is used as a damage parameter. The observed differences between the two materials are less important for low cycle fatigue regime than for high cycle fatigue.

Crack propagation data

This paper also compares the crack propagation behaviours between the BM, the WM and the HAZ. Three stress ratios were investigated: $R_\sigma = 0.0$, $R_\sigma = 0.5$ and $R_\sigma = 0.7$. The last stress ratio was only considered for the BM and WM. Figures 6–9 present experimental crack propagation

Table 2 Constants for the strain-life relations of the BM and WM

Constants	Base material			Welded material		
	$R_\varepsilon = -1$	$R_\varepsilon = 0$	$R_\varepsilon = -1 + R_\varepsilon = 0$	$R_\varepsilon = -1$	$R_\varepsilon = 0$	$R_\varepsilon = -1 + R_\varepsilon = 0$
σ'_f (MPa)	1087.6	923.4	1005.5	1128.6	1026.0	1067.0
b (-)	–0.1090	–0.0955	–0.1033	–0.1086	–0.0958	–0.1007
R^2	0.9641	0.8611	0.9140	0.9854	0.9839	0.9827
ε'_f (-)	0.4108	0.2933	0.3678	4.9545	1.0249	3.7473
c (-)	–0.5547	–0.5311	–0.5475	–1.0017	–0.8119	–0.9805
R^2	0.9918	0.9695	0.9795	0.9826	0.9540	0.9413
$2N_T$	17,344	14,500	16,500	2,042	1,725	1,807
$\Delta\varepsilon_T/2$ (%)	0.365	0.361	0.360	0.481	0.245	0.489

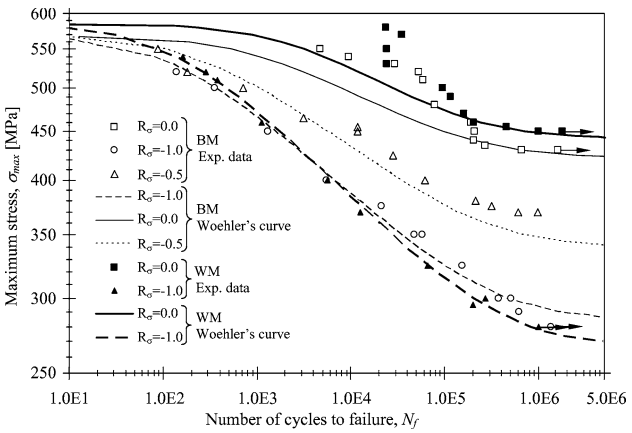

Fig. 4 Stress-life data and Woehler's correlations for BM and WM

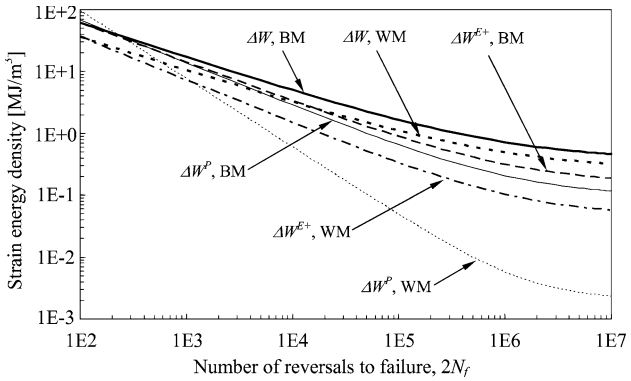

Fig. 5 Comparison of the energy-life relations between the BM and WM

Table 3 Constants required for the description of the Woehler's curves according to Eqs. 4 and 5

Constants	BM	WM
η	6.2	5.6
B_0 (MPa)	1561.6	1785.7
β (1/MPa)	0.001209	0.000779
σ_{l0} (MPa)	284.2	267.4
σ_{UTS} (MPa)	568.11	585

curves. Table 5 summarizes the constants resulting from the best fit of the Paris and Walker equation to the experimental data. Results show that for null stress ratio (Fig. 6) the BM has higher crack propagation rates than WM and HAZ. For a stress ratio equal to 0.5 (Fig. 7) the three materials exhibit very similar behaviours, however is possible to detect a slightly higher crack propagation rate for the BM. Figure 8 enforces the idea of higher crack propagation rate for the BM. The BM and HAZ exhibit very similar crack propagation behaviours for all stress ratios considered. One possible explanation for the higher crack growth rate observed in the BM is the fact that this material exhibits an oriented microstructure resulting from the plate rolling process. The crack was machined in the rolling direction which assists the crack propagation. The material microstructure orientation is partially destroyed for the HAZ (partial re-crystallization) reducing slightly the crack growth rate. The WM exhibits a completely new microstructure without the preferential orientation observed in the BM, which leads to the lowest crack propagation rates.

The increase of the stress ratio produces an increase on crack propagation rates as demonstrates Fig. 9 for the BM. The Walker relation is able of describing the effect of the stress ratio.

The crack propagation tests generated crack growth data covering, essentially, the region II of propagation. In this region the crack propagation data shows a linear relationship as demonstrated by the results of Figs. 6–9. The influence of the stress ratio is less pronounced in region II, than in propagation regions I and III. In fact, the analysis of Fig. 9 shows a small influence of stress ratio on crack growth data. Similar behaviours were observed for the WM and HAZ. Also, it has been demonstrated that materials microstructure has small influence in region II fatigue

Table 4 Constants for the energy-life relations for the BM and WM

Constants	BM	WM
k^P (MJ/m^3)	1671.5	15544.7
α^P	–0.695	–1.105
ΔW_0^P (MJ/m^3)	0.094	0.002
k (MJ/m^3)	787.9	431.7
α	–0.557	–0.542
ΔW (MJ/m^3)	0.361	0.249
k^t (MJ/m^3)	1163.8	918.2
α^t	–0.640	–0.700
ΔW_0^t (MJ/m^3)	0.149	0.046

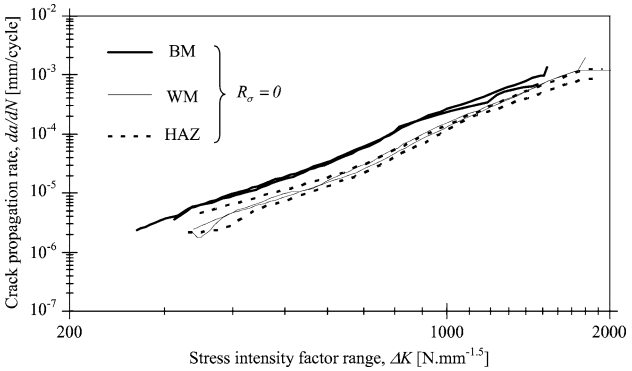

Fig. 6 Comparison of the da/dN vs. Δ K data between the BM, WM and HAZ for R_σ=0

crack growth [33, 34]. This is not true for region I—the near threshold region. This conclusion is verified in this research since the overall scatter band for all data (materials and stress ratios) was narrow. It is interesting to note that results presented in reference [34] correspond to investigations performed using pressure vessels weldments as was done in this work.

In this research no residual stress measurements were performed on CT specimens. The authors believe that

Table 5 Crack propagation constants according to the Paris's law for BM, WM and HAZ

Material	R_σ	m	C	R^2	λ
BM	0.0	3.499	7.195E-15	0.996	0.92
	0.5	3.555	6.281E-15	0.984	
	0.7	3.003	2.037E-13	0.985	
WM	0.0	3.905	2.615E-16	0.994	0.78
	0.5	3.192	5.199E-14	0.991	
	0.7	3.156	6.104E-14	0.981	
HAZ	0.0	3.673	1.141E-15	0.984	0.67
	0.5	2.975	2.258E-13	0.997	

da/dN: mm/cycle; K: N.mm$^{-1.5}$

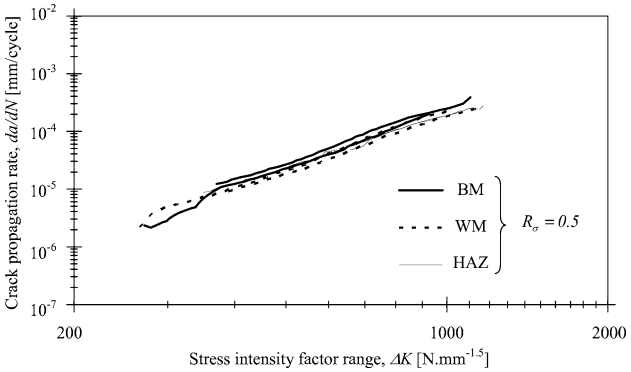

Fig. 7 Comparison of the da/dN vs. Δ K data between the BM, WM and HAZ for R_σ=0.5

eventual residual stresses introduced by the welds were minimized since the specimens were cut from a larger plate and welds were flush ground and their dimensions resulted relatively small. These conditions promote the residual stresses relief. However, if residual stresses persists they should be typically positive, which promotes the crack opening, making the crack propagation rates more insensitive to the stress ratio.

The analysis of the Figs.6–8 suggests that the WM and HAZ have slightly higher fracture toughness than the BM due to the verified higher stress intensity factor range at failure. This conclusion seems to be contradictory with the fact that the WM and HAZ exhibit higher hardness and tensile strengths than the BM. However, the microstructure of the materials can have a determinant influence on the fracture toughness. The fracture toughness is generally more sensitive than other mechanical properties to anisotropy introduced by processing such as the rolling. Since the cracks of the CT specimens were introduced in the rolling direction of the BM this can be responsible for lower fracture toughness of the BM. More robust conclusions about the toughness of the material should be supported by specific toughness tests.

Conclusions

A comparison between the low and high cycle fatigue behaviours of a BM—the P355NL1 steel—and a WM resulting from the automated submerged arc welding was carried out based on stress- and strain-controlled fatigue tests of smooth specimens. A comparison of the crack propagation behaviours between the BM, WM and HAZ was also performed using results from fatigue tests of cracked specimens. The comparisons evidenced some distinct behaviours between the materials considered, which justifies a special attention by engineers concerned with the application of the local approaches plus LEFM to

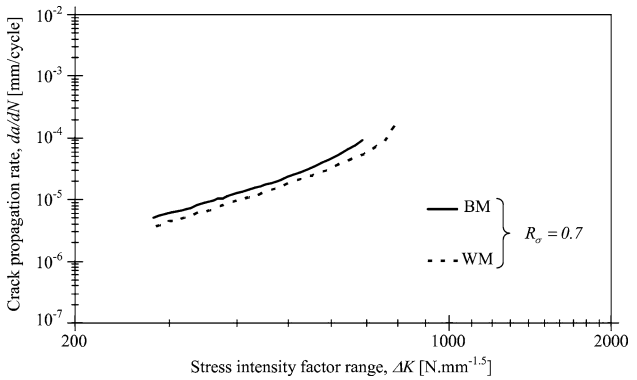

Fig. 8 Comparison of the da/dN vs. Δ K data between the BM and WM for $R_\sigma = 0.7$

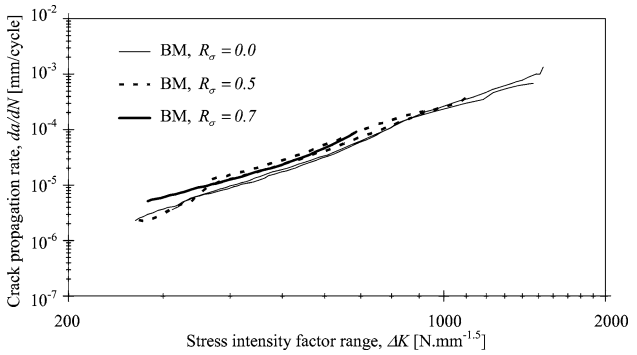

Fig. 9 Comparison of da/dN vs. ΔK data for BM under $R_\sigma = 0$, $R_\sigma = 0.5$ and $R_\sigma = 0.7$

assess welded details. The following main conclusions can be stated:

- Strain-life data was obtained for BM and WM covering two strain ratios namely $R_\varepsilon = 0$ and $R_\varepsilon = -1$. The strain ratio has negligible influence on strain-life behaviour for the two materials. The BM and WM present similar fatigue strength behaviours which justify same fatigue endurance limits. The fatigue ductility behaviours are clearly distinct between the BM and WM. However, this discrepancy only produces a relative small scatter on the global strain-life data. Extrapolations for very low cycle fatigue regions foresee important differences between the fatigue behaviour of the two materials. More experimental data is required in order to increase the confidence of the proposed data for this domain.
- Stress-life relations were proposed based on stress-controlled fatigue data. The representation of Woehler's curves proposed by Lemaitre and Chaboche fairly describes the data in all fatigue domains. The proposed relation encounters some difficulties for null stress ratio and higher maximum stresses. The fully-reversed data indicates similar behaviours for the BM and WM with the exception of the fatigue endurance domain. These conclusions can be extended for null-stress ratio data.
- Energy-life relations were derived from the strain-life data. These relations indicate that the fatigue resistance of the WM, defined in terms of the strain energy density of the cycle, is lower than observed for the BM.
- The BM presents slightly higher crack growth rates than WM and HAZ, for null stress ratio. For stress ratios equal to 0.5 and 0.7 the differences between crack growth rates are almost negligible. The influence of stress ratio is small. In general, crack growth rates obtained for the three materials (three distinct micro-structures) and stress ratios fall in a narrow band, which is in agreement with results published in literature for this type of materials and weldments.

The information provided in this paper (Part II) can be very useful for designers concerned with the assessment of the fatigue behaviour of welded joints of pressure vessels or pressure vessel type details, since it gives several types of fatigue damage laws. In a Part I paper [12], the authors present information required for the evaluation of the damage parameters for the studied materials.

References

1. Taylor N et al (2001) Pressure components fatigue design in the framework of directive 97/23/EC on pressure equipment, Final Report EC DG-ENTR
2. EUROPEAN COMMISSION, Pressure components fatigue design in the framework of directive 97/23/EC on pressure equipment (2001), Final Report DG-JRC/IAM, http// www.ped.eurodyn.com, as on 10 June 2005
3. ASME Boiler and Pressure Vessel Code—Section VIII: Rules for Construction of Pressure Vessels, Division 2 – Alternative rules, Appendix 5: Design Based on Fatigue Analysis, ASME Standards (2001)
4. PD 5500—Specifications for Unfired Fusion Welded Pressure Vessels, British Standards (2003)
5. Unfired Pressure Vessels, European Standards 13445 (2002)
6. Radaj D, Sonsino CM (1998) Fatigue assessment of welded joints by local approaches. Abington Publishing, Abington, UK
7. Tricoteaux A, Fardoun F, Degallaix S, Sauvage F (1995) Fatigue Fract Eng Mat Struct 18:189
8. De Jesus AMP (2004) PhD Thesis, University of Trás-os-Montes e Alto Douro, Portugal
9. Dijkstra OD, Snijder HH, Overbeeke JL, Wildschut H (1987) In: Proceedings of the SIMS'87 conference, Delft, The Netherlands
10. Dijkstra OD, van Straalen IJJ, Noordhoek C (1993) In: Proceedings of the OMAE '93 conference, Glasgow, Scotland
11. De Jesus AMP, Ribeiro AS, Fernandes AA (2006) J Press Vess Technol 128:298
12. De Jesus AMP, Ribeiro AS and Fernandes AA (2006) Soldagem Insp 11:222
13. Coffin LF (1954) Transl ASME 76:931
14. Manson SS, National Advisory Committee for Aeronautics – NACA (1953), Technical Report No.1170
15. Basquin OH (1910) Proc ASTM 10:625
16. Morrow JD, in Internal Friction, Damping and Cyclic Plasticity, ASTM, Philadelphia, 1965, p.45, ASTM STP 378

17. Lemaitre J, Chaboche JL (1990) Mechanics of solid materials. Cambridge University Press, Cambridge UK
18. Halford GR (1966) J Mater 1:3
19. Lefebvre D, Ellyin F (1984) Int J Fatigue 6:9
20. Ellyin F, Kujawski D (1984) J Press Vess Technol 106:342
21. Golos K, Ellyin F (1988) J Press Vess Technol 110:36
22. Ellyin F (1997) Fatigue damage, crack growth and life prediction. Chapman & Hall, London, UK
23. Ribeiro AS (1993) PhD Thesis, University of Trás-os-Montes and Alto Douro, Portugal
24. Sanford RJ (1997) Selected papers on foundations of linear elastic fracture mechanics - Volume CP1. SEM Classic Papers, Bethel, Connecticut, USA
25. Paris PC, Gomez MP, Anderson WE (1961) Trend Eng 13:9
26. Paris PC, Erdogan F (1963) J Basic Eng 85:528
27. Walker EK (1970) in Effects of environment and complex load history on fatigue life, ASTM, Philadelphia, 1970, ASTM STP 462
28. Hoeppner DW, Krupp WE (1974) Eng Fract Mechanics 6:47
29. Flat Products Made of Steels for Pressure Purposes - Part 3: Weldable Fine Grain Steels, Normalized, European Standards 10028–3 (2003)
30. Weldable Normalized Fine Grain Structural Steels. Technical Delivery Conditions for Plate, Strip, Wide Flats, Sections and Bars, Deutsche Norm 17102 (1983)
31. Standard Practice for Strain-Controlled Fatigue Testing, ASTM standards E606-92 (1998)
32. ASTM, American Society for Testing and Materials (1999) ASTM E647: standard test method for measurement of fatigue crack growth rates, in Annual Book of ASTM Standards, Vol. 03.01, ASTM, West Conshohocken, PA, pp 591–629
33. Maddox SJ (1974) Weld J 53:401
34. James LA (1977) Weld J 56:386